JOURNAL OF SPACECRAFT AND ROCKETS
Vol. 43, No. 4, July–August 2006

Effect of Computational Method on Discrete Roughness Correlations for Shuttle Orbiter

Scott A. Berry,* H. Harris Hamilton II,† and Kathryn E. Wurster‡
NASA Langley Research Center, Hampton, Virginia 23681

A reanalysis of discrete roughness boundary-layer transition data using a consistent computational method for comparison to other published results has been completed. The primary objective of this effort was to investigate the influence of the computational approach on the resulting transition correlation. The experimental results were previously obtained on Space Shuttle Orbiter models in the NASA Langley Research Center 20-Inch Mach 6 Air Tunnel. The phosphor thermography system was used to monitor the status of the boundary layer via global heat-transfer images of the orbiter windward surface. The existing roughness transition database included a variation in the size and location of discrete roughness trips along the centerline of 0.0075-scale models at an angle of attack of 40 deg. Various correlative approaches were attempted, with the roughness transition correlations based on edge properties providing the most reliable results. When a consistent computational method is used to compute edge conditions, transition data sets for different moderately blunt configurations at several angles of attack are shown to collapse to a well-behaved correlation. The shuttle experimental dataset presented herein, therefore, can be used to calibrate the preferred computational method of the end user for use in the future designs of the next-generation space access vehicles.

Nomenclature

H	=	enthalpy, Btu/lbm
h	=	heat-transfer coefficient (lbm/ft^2-s), $= q/(H_{aw} - H_w)$, where $H_{aw} = H_{t2}$
$h_{F\text{-}R}$	=	reference coefficient using Fay–Ridell calculation to stagnation point of a sphere
k	=	roughness element height, in.
L	=	model reference length from nose to body-flap hinge line (9.7 in)
M	=	Mach number
p	=	pressure, psi
q	=	heat-transfer rate, Btu/ft^2-s
Re	=	unit Reynolds number, 1/ft
Re_k	=	roughness Reynolds number based on height k and conditions at k
Re_{ke}	=	roughness Reynolds number based on height k and edge conditions
Re_L	=	length Reynolds number based on L
Re_θ	=	momentum thickness Reynolds number
T	=	temperature, °R
x	=	longitudinal distance from the nose, in.
α	=	model angle of attack, deg
δ	=	boundary-layer thickness, in.
θ	=	momentum thickness, in.

Subscripts

aw	=	adiabatic wall
e	=	local edge condition
eff	=	effective
inc	=	incipient
tr	=	transition onset
$t1$	=	reservoir conditions
$t2$	=	stagnation conditions behind normal shock
w	=	model surface
∞	=	freestream static conditions

Presented as Paper 2002-2744 at the AIAA 32nd Fluid Dynamics Conference, St. Louis, MO, 24–27 June 2002; received 15 September 2003; accepted for publication 29 November 2005.

*Aerospace Engineer, Aerothermodynamics Branch, Research and Technology Directorate. Member AIAA.

†Visiting Researcher; currently Researcher, Department of Mechanical and Aerospace Engineering, North Carolina State University, c/o NASA Langley Research Center, Hampton, VA 23681.

‡Aerospace Engineer, Vehicle Analysis Branch, Systems Analysis and Concepts Directorate. Associate Fellow AIAA.

Introduction

THE Space Shuttle Orbiter represents the current state of the art in reusable launch vehicles (RLV), despite the fact that it was designed and built over 25 years ago. Recently, NASA's new Vision for Space Exploration has set the date for shuttle replacement with the next-generation space vehicle, a return to the Apollo-era blunt capsule. The aging orbiter fleet is currently planned for retirement by 2010. The orbiters, therefore, are likely to be the only vehicles available in the near term to obtain valuable aerothermodynamic and boundary-layer transition flight data, which can be used to minimize design uncertainties for the next-generation RLV or space access vehicle.

Early in the design process of the Space Shuttle Orbiter, boundary-layer transition was recognized to be a significant aerothermodynamic challenge.[1] The aerothermodynamic database that was developed before the first flight of the orbiter in 1981 resulted from more than 12 years of testing in many of the major U.S. ground-based facilities. This database development was prior to the availability of computational fluid dynamics (CFD) capabilities. Consequently, wind tunnels were heavily used to define the boundary-layer transition criteria that would predict when during reentry the vehicle would transition from laminar to turbulent flow and the resulting increase in heating to the vehicle. The resulting wind-tunnel-derived transition criteria were thought to be conservative (because of the influence of tunnel-noise contamination associated with conventional facilities), and this was essentially validated when the orbiter eventually flew.[1] However, the orbiter occasionally experiences boundary-layer transition much earlier in the trajectory as a result of surface roughnesses[2] that result from the relatively fragile nature (as dramatically demonstrated recently on *Columbia*) of the thermal protection system (TPS). The orbiter typically suffers launch-induced damage to the TPS (gouges in the tiles from ice and other debris falling off the tank at liftoff) and occasional protrusions of the tile gap fillers that can lead to early transition during the reentry. The random nature of this roughness results in a wide range of freestream conditions (Mach numbers between 6 and 18 and length Reynolds numbers between 2.5 and 13×10^6) at which transition

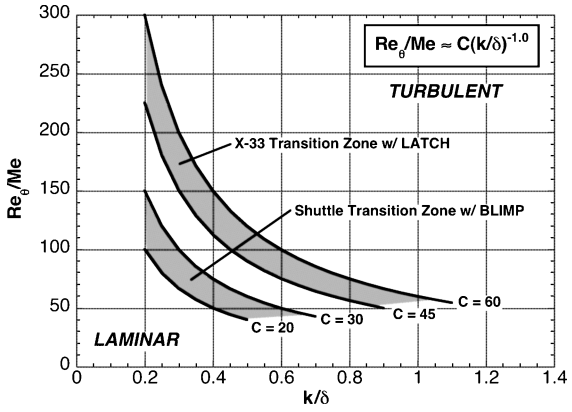

Fig. 1 Comparison of published orbiter[3] and X-33 (Ref. 4) results.

occurs in flight. The conservative design philosophy that was utilized for the orbiter has compensated for the occasional early transition results thus far. However, for next-generation RLVs, in which design margins will need to be reduced to enhance payload capability, a more reliable transition prediction capability will be required.

To help reduce uncertainties associated with hypersonic boundary-layer transition, a study of roughness effects on the orbiter has been ongoing at NASA Langley Research Center (LaRC). A ground-based investigation of roughness-induced transition on the Space Shuttle Orbiter was conducted at LaRC, and the results were subsequently published in Refs. 2 and 3. The resulting transition data show that a simple approach for correlating roughness transition data utilizing the momentum thickness Reynolds number divided by the edge Mach number (Re_θ/M_e) and the boundary-layer trip height divided by the boundary-layer thickness (k/δ) accurately predicts onset of transition. The calculated boundary-layer parameters were originally obtained using the BLIMP code (not publicly available). All of the data, from wind tunnels at LaRC and Arnold Engineering and Development Center (AEDC) Tunnel B, as well as flight, were compared based on boundary-layer parameters computed from this same code.[2] Since then, additional boundary-layer transition studies for the X-33[4] and X-38[5] programs were conducted at LaRC; however, the LATCH[6] code was used to calculate the boundary-layer parameters. Although the wind-tunnel transition results from the X-33 and X-38 studies correlated well using the Re_θ/M_e vs k/δ approach, the results did not agree with the orbiter correlation developed with BLIMP code. Figure 1 shows that the orbiter and X-33 correlations differ by a factor of two.

A recent paper on roughness-dominated transition correlations[7] reviewed several published results in an attempt to unify the different correlation methods and results. The author, however, acknowledged that the differences inherent within the various computational approaches were not accounted for. Uncertainties in flowfield calculations associated with a transition study will directly influence the uncertainty of the correlation method.[8] For example, different computational methods can provide significant differences in the calculated edge properties used in the correlations, as noted in Refs. 9 and 10. The present paper, therefore, compares the orbiter and X-33 results using a consistent computational approach. In summary, the objectives of this paper are to investigate the influence of the computational method on the development of discrete roughness correlations, to compare various roughness-dominated transition datasets based on a consistent approach, and to examine alternate correlation approaches. Finally, once the credibility of the present data set is established, the discrete roughness transition criteria will be reexamined using a relatively simple and well-known engineering method, the MINIVER code. The present data set can also be used to calibrate the preferred computational technique of the future designers of the next-generation RLV.

Transition Correlations

In the mid-1950s, the dawning of the ballistic missile era brought forth the first concerns over boundary-layer transition at hypersonic conditions.[8] Over the years hypersonic vehicle concepts have changed dramatically, starting with the blunt ballistic vehicles, then the moderately blunt lifting bodies, and recently the slender airbreathing configurations. The approaches that different researchers have used over the years to correlate empirically derived transition results have also changed. However, during the past 50 or so years of research, no universal transition correlation method has yet to be identified that can predict transition in flight for all classes of vehicles.

Initially, the focus for boundary-layer research was on blunt configurations and in particular the problem of nose-tip transition. Many references that discuss the importance of surface roughness in the subsonic portion of the nose cone (far too numerous to site all here) are available. Reference 11 provides an overview of the early work on nose-tip transition relevant to blunt ballistic vehicles. In particular the large database provided by the Passive Nosetip Technology (PANT) program is reviewed. Much of the nose-tip work focused on the problem of distributed surface roughness that develops from ablating nose cones. The surface ablation, which usually is driven by the early laminar conditions, causes the formation of microroughness patterns that are dependent upon the material composition and fabrication process. The large body of work on nose-tip transition led to the concept of the critical roughness Reynolds number Re_k approach for blunt bodies in hypersonic flow.[7] This approach requires detailed computations of the flowfield within the boundary layer, as Re_k is based on local conditions at the top of the trip at the location of transition onset (in the case of distributed roughness). Because of the time and effort required to obtain high-quality boundary-layer profiles for a wide range of flow conditions, many researchers have simplified this approach by using conditions at the boundary-layer edge instead of the trip height to calculate a modified roughness Reynolds number Re_{ke} (for instance, see Ref. 12).

In the early 1980s, research efforts shifted to include moderately blunt lifting-body vehicles, like the Space Shuttle Orbiter. Boundary-layer transition on these vehicles tends to occur further back on the vehicle where the boundary-layer edge is mostly supersonic. Much of the transition database that was obtained for the orbiter program prior to the first flight was to define the distributed surface roughness limit for the vehicle that would allow it to still be considered "aerothermodynamically smooth." Based on the orbiter design philosophy, a smooth surface was defined as a surface whose roughness did not promote transition earlier than predicted using conservative wind-tunnel-derived correlations.[1] An average distributed roughness of the order of 0.05 in. on the full-scale orbiter represented a smooth vehicle, based on postflight analysis.[2] The remainder of the orbiter transition database was dedicated to understanding the effect of isolated (discrete) three-dimensional roughness elements that exceed the distributed roughness limit. Van Driest and Blumer[12] developed a roughness transition correlation based on edge conditions using spherical trips on a sharp cone in a supersonic wind tunnel. A postflight analysis of the STS-1 to 5 flights shows that this correlation correctly predicts transition onset near the orbiter nose. On flights in which transition occurred significantly early because of protruding gap fillers (STS-28 and 73, for instance), the estimated roughness heights[2] exceeded the minimum required effective height based on the Van Driest and Blumer correlation. (It should be noted that the actual dimensions of the protruding gap fillers are not known during the flight, but must be estimated based on postflight inspections.) For future lifting-body RLV designs (orbiter-like configurations), if the distributed surface roughness is minimized, for instance, through the use of a robust metallic TPS, transition behavior in flight will most likely be influenced by discrete roughness elements.

To compare and contrast different transition correlations, the boundary-layer parameters must be obtained via a reliable and appropriate computational method. Reference 13 provides an extensive list of possible transition correlations. The present paper will judiciously select a moderate subset (influenced by the parameters available from the choice of computational method) of the transition correlation approaches that have been attempted over the past 50 years. As noted in Ref. 7, a power-law relationship between an

assumed disturbance parameter (usually related to the roughness height) and an assumed transition parameter (usually related to the local conditions within the calculated laminar boundary layer) is typically sought. A lot of the orbiter work has been based on the selection of Re_θ/M_e as the transition parameter.[1] Also, the disturbance parameter has typically been based on the trip height referenced by boundary-layer edge properties (boundary layer or momentum thickness) or by Re_k.

Boundary-layer properties used for development of transition correlations can be obtained from computational methods of differing complexity and sophistication. The simplest methods to implement are based on engineering codes (for example, MINIVER[14]), which, typically, provide boundary-layer edge properties, but not the properties within the boundary layer that are required to formulate the Re_k parameter. More sophisticated codes that solve the differential form of the boundary-layer equations are required to obtain Re_k values, however at the expense of additional computational time and resources. Viscous Navier–Stokes (NS) solutions could also provide all of the necessary properties, but with the added complexity of grid-sensitivity issues associated with the proper derivation of the boundary-layer edge.[8] Typically, for any given study or program, both the time and the computational resources available limit the number of detailed NS solutions that can be obtained. Instead coupled inviscid/boundary-layer and/or engineering methods are heavily used to augment the computational domain. Recent experience at NASA for the X-34 program, for example, shows that, based on the computational resources available within the program schedule, detailed laminar NS solutions were completed at flight conditions for only two points along the trajectory.[15] At the same time, six flight cases were computed using an inviscid/boundary-layer approach,[16] while the entire flight trajectory was computed with an engineering code,[17] albeit for a limited number of locations on the vehicle (approximately 100 body points). The increased productivity associated with the approximate methods might be more conducive for additional computations for the wind-tunnel cases necessary for development of a calibrated, but code-specific, transition correlation. Additionally, a transition correlation appropriate to a highly productive engineering code such as MINIVER could facilitate the integration of transition concerns into the real-time entry trajectory development. For large-scale entry vehicle concepts with reusable TPS, delay of transition onset until the nominal heating levels are well below peak heating to the successful achievement of an optimal TPS/trajectory combination. To date, an Re_θ/M_e criterion is typically used for such efforts.[18] The transition value chosen is loosely coupled to the geometry. A correlation developed in the manner described herein would add a level of fidelity not currently available and could be more closely coupled to the vehicle configurations under consideration.

Experimental Method

Test Facility

The present experimental discrete roughness results, originally published in Ref. 3, were obtained in the LaRC 20-Inch Mach 6 Air Tunnel. Miller[19] provides a detailed description of this blowdown facility. Typical operating conditions for the tunnel are stagnation pressures ranging from 30 to 500 psia, stagnation temperatures from 760 to 940°R, and freestream unit Reynolds numbers from 0.5×10^6 to 8×10^6 per foot. A two-dimensional, contoured nozzle is used to provide nominal freestream Mach numbers from 5.8 to 6.1. The test section is 20.5×20 in.; the nozzle throat is 0.399×20.5 in. A bottom-mounted model injection system can insert models from a sheltered position to the tunnel centerline in less than 0.5 s. Run times up to 15 min are possible with this facility, although for the current heat-transfer and flow visualization tests, the model was exposed to the flow for only a few seconds. Flow conditions were determined from the measured reservoir pressure and temperature and the measured pitot pressure at the test section and were compared to a recent unpublished calibration of the facility.

Test Techniques

The two-color relative-intensity phosphor thermography technique is now routinely being applied to aeroheating tests in the hypersonic wind tunnels of LaRC. Details of the phosphor thermography technique are provided in Refs. 20–22. References 3, 4, and 5 are recent examples of the application of this technique to wind-tunnel testing. The primary advantage of phosphor thermography is the global resolution of the quantitative heat-transfer data. Such data can be used to identify the heating footprint of complex, three-dimensional flow phenomena (e.g., transition fronts, turbulent wedges, boundary-layer vortices, etc.), which are extremely difficult to resolve by discrete measurement techniques. Phosphor thermography is routinely used in Langley's hypersonic facilities as quantitative global surface heating information is obtained from models that can be fabricated quickly (a few weeks) and economically (an order of magnitude less than the thin-film technique). Recent comparisons of heat-transfer measurements obtained from phosphor thermography to conventional thin-film resistance gauges (Ref. 23) and CFD predictions (Refs. 24 and 25) show excellent agreement.

Model Description

Cast ceramic 0.0075-scale Space Shuttle Orbiter models were built in accordance with the procedures detailed in Ref. 26. The models are coated with a mixture of phosphors suspended in a silica-based colloidal binder. This coating consists of a 5:1 mixture of lanthanum oxysulfide (La_2O_2S) doped with trivalent europium and zinc cadmium sulfide (ZnCdS) doped with silver and nickel. The coatings typically do not require refurbishment between runs in the wind tunnel and have been measured to be approximately 0.001 in. thick. The final step in the fabrication process is to apply fiducial marks along the body to assist in determining spatial locations accurately. The fiducial marks, in this case, were applied at locations that correspond to the roughness element locations. These locations were identical to the trip locations used in Ref. 27 with the exception of the two additional centerline locations at DE and ECL. Table 1 provides a list of the fiducial marks used for the present investigation, while Fig. 2 provides a sketch of these trip locations and shows details of the trip dimensions.

The roughness elements simulate a raised TPS tile, as discussed in Ref. 3. The trips were cut from 0.0025-in.-thick polyimide tape and variations on the roughness heights k were obtained by stacking multiple layers of tape (heights of 0.0025, 0.005, 0.0075, and 0.010 in. were used). The trip designation used for the present study utilizes the station name followed by the number of layers (for instance, B2 identifies a 0.005-in. trip at station B).

Test Conditions

The range of freestream unit Reynolds numbers Re, of 0.5 to 8.0×10^6 per foot, corresponds to a length Reynolds number Re_L of approximately 0.4 to 6.7×10^6 on the 0.0075-scale model. The upper bound is within in the general range of Re_L in flight at the time of transition.[2] To obtain roughness transition data, the unit Reynolds number was systematically varied for each trip height and location

Table 1 Fiducial marks and trip locations

Trip	x/L	y/L
A	0.050	0.00
B	0.070	0.00
C	0.070	0.011
D	0.090	0.00
DE	0.174	0.00
ECL	0.258	0.00
E	0.258	0.015
F	0.258	0.039
G	0.375	0.00
H	0.375	0.033
I	0.375	0.053
J	0.575	0.00
K	0.620	0.133

Table 2 Nominal flow conditions and run-to-run repeatability for 20-Inch Mach 6 Air Tunnel

$Re_\infty(\times 10^6/\text{ft})$	M_∞	P_{t1}, psi	T_{t1}, °R	H_{t1}, Btu/lbm	P_{t2}, psi
0.59 ± 4.6%	5.84 ± 0.03%	29.8 ± 4.4%	861.7 ± 0.3%	207.2 ± 0.3%	0.99 ± 4.2
0.88 ± 2.1%	5.86 ± 0.03%	44.8 ± 2.9%	865.9 ± 0.9%	208.2 ± 1.0%	1.47 ± 2.8
1.15 ± 3.3%	5.88 ± 0.05%	60.3 ± 3.8%	880.8 ± 0.5%	212.0 ± 0.5%	1.95 ± 3.7
1.58 ± 2.6%	5.90 ± 0.03%	84.7 ± 2.4%	889.7 ± 0.8%	214.2 ± 0.8%	2.69 ± 2.2
1.86 ± 1.7%	5.92 ± 0.03%	100.1 ± 2.2%	887.6 ± 0.3%	213.5 ± 0.7%	3.14 ± 2.1
2.23 ± 1.8%	5.94 ± 0.02%	125.1 ± 1.4%	906.7 ± 0.7%	218.2 ± 0.7%	3.88 ± 1.3
2.73 ± 1.7%	5.95 ± 0.01%	154.7 ± 1.0%	909.1 ± 0.5%	218.8 ± 0.5%	4.74 ± 0.9
3.16 ± 2.4%	5.96 ± 0.02%	180.3 ± 1.6%	909.9 ± 0.8%	219.0 ± 0.9%	5.48 ± 1.5
3.79 ± 0.8%	5.98 ± 0.00%	217.0 ± 0.1%	909.1 ± 0.5%	218.8 ± 0.5%	6.54 ± 0.1
4.40 ± 2.3%	5.98 ± 0.01%	250.7 ± 1.1%	906.2 ± 1.0%	218.1 ± 1.1%	7.52 ± 1.1
4.87 ± 3.2%	5.99 ± 0.01%	292.2 ± 0.7%	933.3 ± 1.5%	224.8 ± 1.6%	8.73 ± 0.7
5.41 ± 1.6%	6.00 ± 0.01%	325.6 ± 0.6%	934.1 ± 0.9%	225.0 ± 0.9%	9.69 ± 0.6
5.81 ± 3.0%	6.00 ± 0.03%	348.7 ± 3.0%	931.8 ± 0.5%	224.4 ± 0.5%	10.35 ± 2.9
6.73 ± 1.8%	6.01 ± 0.02%	401.7 ± 1.4%	926.6 ± 0.4%	223.1 ± 0.4%	11.85 ± 1.3
7.95	6.02	475	925	222.6	13.88

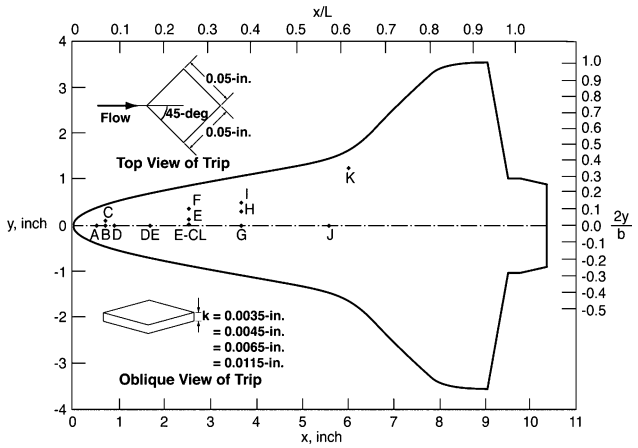

Fig. 2 Sketch of 0.0075-scale orbiter windward surface showing fiducial mark locations and details of the trips.

to obtain the incipient, critical, and effective Reynolds numbers. Note that the present terminology is similar to the definitions of Bertin et al.[28] except that Reynolds number has been substituted for trip height. Van Driest and Blumer,[12] Boudreau,[29] and Pate[30] discuss trip effectiveness as a function of Reynolds number, but without the use of these specific terms. And whereas Boudreau defined effectiveness based on the end of transition, transition onset is used for the present study (following Bertin). The incipient Reynolds number was identified, based on the heating distributions, as the maximum Reynolds number at which laminar flow was maintained behind the trip. The critical Reynolds number corresponds to the Reynolds number where significant nonlaminar flow first appears downstream of the roughness element. The effective Reynolds number was identified by the minimum Reynolds number where the transition front appears fixed at or near the roughness element. Generally, the Reynolds-number increment from run to run was on the order of 0.5×10^6 per foot. Typically, the incipient, critical, and effective values of Reynolds number would be identified within three successive runs in the tunnel. The angle of attack is 40 deg, and the sideslip is zero for all of the runs presented herein.

Data Reduction

Heating rates were calculated from the global surface temperature measurements using one-dimensional semi-infinite solid heat-conduction equations, as described in Refs. 20 and 21. Based on considerations presented in Ref. 20, phosphor system measurement error is believed to be less than ±8%, with overall experimental uncertainty of ±15%. Heating distributions are presented in terms of the ratio of heat-transfer coefficients $h/h_{\text{F-R}}$, where $h_{\text{F-R}}$ corresponds to the Fay and Ridell[31] stagnation-point heating to a sphere with radius 0.09 in. (a 1-ft radius sphere scaled to the model size). Repeatability of the centerline heat-transfer distributions was found to be generally better than ±4%.

Computational Methods

LATCH

The engineering code LATCH (Langley Approximate Three-Dimensional Convective Heating)[6] was used to obtain the primary set of boundary-layer edge properties for the present paper. This approximate method for three-dimensional bodies has been validated against both experimental and computational results. LATCH is based on the axisymmetric analog for three-dimensional boundary layers and uses a generalized body-fitted coordinate system to compute edge properties and heating along individual streamlines. Edge conditions for the boundary-layer solution are obtained along the streamlines from an inviscid flowfield calculated by an inviscid version of the LAURA code.[32] Further details of the code can be found in Ref. 6.

For approximate methods, the classical approach of assuming that the boundary-layer edge properties are given by the inviscid wall conditions has been shown to be inappropriate for blunt bodies.[33] With LATCH, the boundary-layer edge properties are typically obtained by interpolating in the inviscid flowfield to a distance equal to the boundary-layer thickness away from the wall. To accomplish this, an initial assumption is made for the boundary-layer edge properties (usually the wall values), and the boundary-layer thickness is then computed. Next the edge properties are recomputed based on this new location within the flowfield, and the solution is iterated until the change in boundary-layer thickness becomes small. Typically two or three iterations are required for convergence. Edge properties determined in this manner account for the effect of variable entropy at the boundary-layer edge. On the other hand, using the inviscid surface conditions as the boundary-layer edge properties corresponds to a constant entropy condition across the boundary layer and allows solutions to be obtained more quickly. A constant entropy assumption will allow for a consistent comparison of the present orbiter results to X-33[4] and X-38[5] results. Thus, for the present paper LATCH was applied using the inviscid wall conditions to obtain the boundary-layer edge properties for the transition correlations based on the nominal unit Reynolds-number (Re) cases listed in Table 2. For the case where incipient and effective transition is observed to occur at a Reynolds number that is between the nominal cases, the transition parameters are interpolated.

Engineering relations are used in LATCH to approximate both the momentum thickness θ and the boundary-layer thickness δ (Ref. 34). The computed surface properties are used to calculate θ and the shape factor, $\delta/\theta = \text{constant}$, is used to obtain δ. Based on the results presented in Ref. 35, the shape factor is primarily a function of wall-to-total temperature; a shape factor of 5.5 is used for cold-wall conditions and 8 for adiabatic conditions. The application of LATCH to orbiter flight cases[6] showed that a shape factor of 5.5 was appropriate for the cold-wall surface conditions of flight.

The transient-based heat-transfer techniques used in wind tunnels also provide cold-wall conditions. For all of the LATCH results compared presently, the shape factor relation $\delta/\theta = 5.5$ was used to estimate the boundary-layer thickness.

SABLE

The SABLE code employs a finite difference technique to solve the steady, compressible, axisymmetric boundary-layer equations for both laminar and turbulent flows. This code has been validated against experimental and computational results.[36] The SABLE solutions, which approximately account for the variable entropy condition, provide boundary-layer profiles and edge properties, based on 99.5% of the edge velocity. The boundary-layer edge properties are compared to the LATCH results, whereas the profile information are used to calculate Re_k.

BLIMP

The previous investigation into shuttle transition correlations utilized computations of flowfield parameters based on a two-layer approach. The two-layer approach used was a three-step process. First, an inviscid flowfield about the orbiter configuration was computed. Second, using the inviscid flowfield as input, a streamline tracing code was used to define the pressure distributions, streamline spreading metrics, and the local boundary-layer edge entropy along the inviscid streamline. Finally, a boundary-layer code was used to compute the surface heating rates and the boundary-layer parameters. The IEC3D inviscid flowfield solver[37] was used to compute the inviscid flowfield for the orbiter at $a = 40$ deg. The streamline code developed by Wang[38] was used to generate the pressure, metric, and the edge entropy distributions along inviscid streamlines. The Boundary Layer Integral Matrix Procedure (BLIMP) code was used to compute the surface heating rates and the boundary-layer parameters using perfect-gas assumptions and a fixed wall temperature of 540°R.

MINIVER

The primary motivation for the present paper was to investigate the influence of the computational method on the development of transition correlations, and as such the engineering code MINIVER,[14] which is heavily used by vehicle designers, was also evaluated. MINIVER is a versatile engineering code that uses various well-known approximate heating methods, together with simplified flowfields and geometric shapes for modeling the vehicle, to perform simple TPS sizings for aerospace vehicles that operate in the hypersonic flight regime. MINIVER is suitable for research at the conceptual and preliminary design level. Postshock and local flow properties based on normal-shock or sharp-cone entropy conditions are determined in MINIVER through user selection of the various shock shape and pressure options. The calculations can be based on perfect-gas or equilibrium-air chemistry. Angle-of-attack effects are simulated either through the use of an equivalent tangent-cone or an approximate crossflow option. The flow can be calculated for either two- or three-dimensional surfaces. However, the three-dimensional effects are available only through the use of the Mangler transformation for flat-plate to sharp-cone conditions. The principle advantage of this engineering code over some of the more detailed methods is the speed with which the analyses can be performed for each flow condition along a trajectory.

Discussion of Results

Computational Comparisons

The transition correlations developed in the present paper are based on the LATCH and SABLE solutions. By comparing the boundary-layer results with these two codes to that previously obtained from the BLIMP code, important differences are highlighted in terms of both the transition and disturbance parameters. The purpose of the comparison is not to suggest which code is more accurate but rather to illustrate the differences that can arise from various codes and the effect of those differences on the resulting transition correlation.

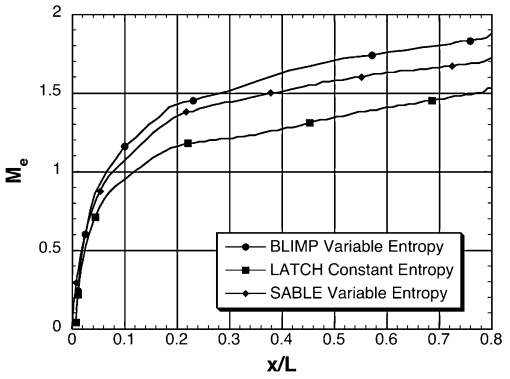

Fig. 3 Comparison of calculated edge Mach-number distributions.

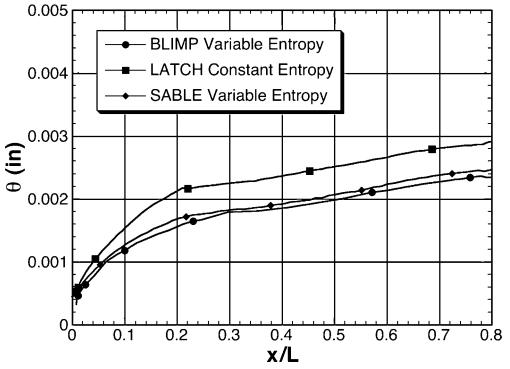

Fig. 4 Comparison of calculated momentum thickness distributions.

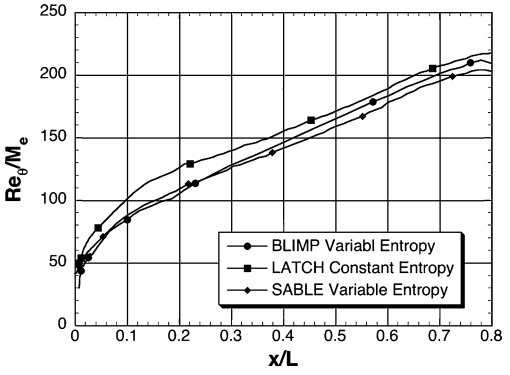

Fig. 5 Comparison of calculated momentum thickness Reynolds number divided by the edge Mach number.

For the transition parameter Re_θ/M_e, LATCH calculates the local Reynolds number, the momentum thickness, and edge Mach number directly. Figure 3 compares the calculated M_e distributions along the centerline from LATCH, SABLE, and BLIMP for the unit Reynolds number $Re = 2.73 \times 10^6$/ft. For the LATCH solution, which as discussed earlier does not account for variable entropy, M_e is 20% lower than the BLIMP results (which does account for variable entropy). The SABLE code, which also calculates the boundary-layer edge parameters based on variable entropy conditions, results in a M_e closer to the BLIMP results. The momentum thickness θ distributions are shown in Fig. 4. In this case, the LATCH results are roughly 20% higher than BLIMP. The variable entropy result from SABLE, however, nearly matches the BLIMP calculations. The differences in the local edge properties appear to be the result of the assumed entropy condition with LATCH and BLIMP. Fortuitously, when these edge properties are used to compute Re_θ/M_e the differences largely cancel out, as shown in Fig. 5. The LATCH result is within 15% of BLIMP, while the SABLE result is almost identical. In this case, even though these computations have significant differences in the edge properties, the transition parameter is actually in fairly good agreement, with the difference between LATCH and BLIMP being less than 15%.

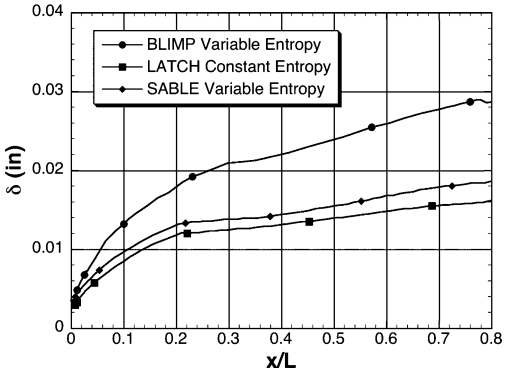

Fig. 6 Comparison of calculated boundary-layer thickness distributions.

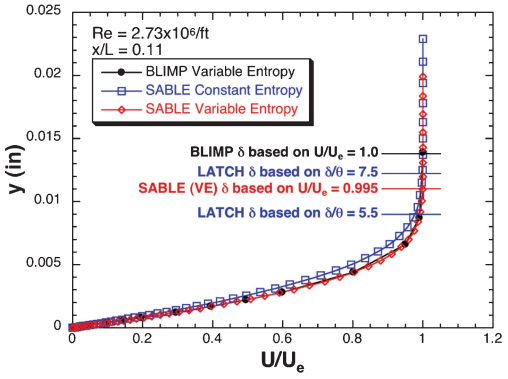

Fig. 7 Sample boundary-layer profile comparison.

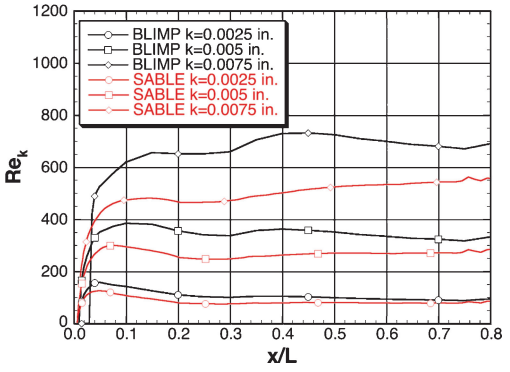

Fig. 8 Comparison of calculated roughness-height Reynolds-number distributions.

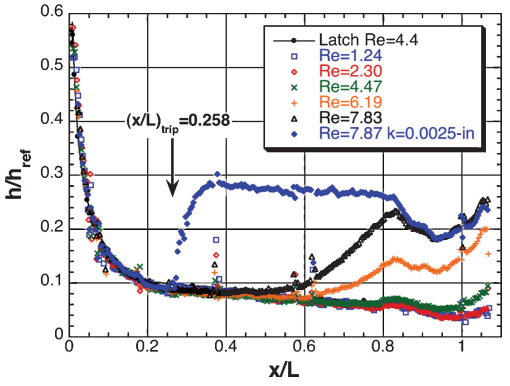

Fig. 9 Comparison of smooth-body and tripped heating distributions for a range of Reynolds number to laminar LATCH prediction.

For the disturbance parameter k/δ, the trip height k is known from the experiment, while the boundary-layer thickness δ is obtained from the computations. For BLIMP, δ is calculated directly from the boundary-layer equations based on $U/U_e = 1$ at the edge. The edge velocity U_e is assumed from a nonisentropic expansion and includes the streamwise variation in entropy. As just discussed, engineering relations[34] are used in LATCH to approximate δ based on a shape factor of $\delta/\theta = 5.5$. Figure 6 provides a comparison between the three codes of the boundary-layer thickness distribution along the centerline for $Re = 2.73 \times 10^6$/ft. In this case, the SABLE results are closer to LATCH, which is unexpected considering the different assumptions and methodologies that are used. However, the difference between the SABLE and BLIMP results can be more significant. Recall that SABLE calculates δ based on 99.5% of the edge velocity, whereas BLIMP uses 100%; thus the difference between the two shown in Fig. 6. Based on a typical boundary-layer profile obtained from BLIMP and shown in Fig. 7, the difference between 99.5 and 100% of the edge velocity results in a nearly 40% difference in the boundary-layer thickness. As for the comparison between BLIMP and LATCH in Fig. 6, the boundary-layer thickness from BLIMP is on the order of 50% larger than LATCH. The difference in the calculated boundary-layer thickness between the two codes appears to be the major source of the discrepancy shown in Fig. 1.

Figure 7 provides a comparison of boundary-layer profiles obtained from both BLIMP and SABLE for $Re = 2.73 \times 10^6$/ft and $x/L = 0.11$. As LATCH does not provide boundary-layer profiles, SABLE was used to compute a constant entropy case representative of LATCH for comparison. Both velocity profiles under variable entropy conditions are nearly identical. The constant entropy case results in a larger boundary-layer thickness. The actual computed δ from BLIMP, LATCH, and SABLE for this location and Reynolds number are also shown in Fig. 7 and shows that the LATCH constant entropy result is smaller than obtained from BLIMP and SABLE because of the use of the shape factor value of 5.5. As discussed earlier, this shape factor in LATCH was determined by comparison to orbiter flight data. The wind-tunnel cases are also typically cool wall; however, the wall-to-total temperature in the tunnel is between flight and adiabatic wall conditions. The SABLE solutions, which calculate both θ and δ directly, show that a shape factor of 7.5 is more appropriate for these wind-tunnel cases. If a shape factor constant of 7.5 is used in LATCH, the calculated boundary-layer thickness would be much closer to the BLIMP results. So although the boundary-layer thickness difference is the major reason for the discrepancy in the correlations results shown in Fig. 1, the reason for the difference is most likely caused by the use of an inappropriate shape factor in LATCH.

For disturbance parameters based on Re_k, the SABLE code was used to obtain the flowfield properties within the boundary layer. The distribution of Re_k along the model centerline based on fixed heights within the boundary layer (corresponding to the first three trip heights, $k = 0.0025$, 0.0050, 0.0075 in. only) from SABLE (based on constant entropy to be consistent with LATCH) and BLIMP for the representative unit Reynolds-number case ($Re = 2.73 \times 10^6$/ft) is shown in Fig. 8. The Re_k values from BLIMP are roughly 30% higher than those from SABLE. Because the boundary-layer thickness results from BLIMP are larger than the SABLE results, a fuller velocity profile would be required in order for the Re_k values from BLIMP to also be larger for a given fixed height within the boundary layer; this is observed in Fig. 7. For instance, for a trip height of $k = 0.005$ in. the velocity within the boundary layer referenced by the edge condition is approximately 6% higher for the BLIMP calculations, and coupled with the different calculated edge velocities (based on constant versus variable entropy conditions), accounts for the nearly 30% difference in Re_k. These differences provide further evidence of the importance of using a consistent computational method when comparing results.

Experimental Results

Figure 9 compares the measured centerline heating distributions for a range of Reynolds number on the smooth model and a sample trip case. Also shown is the laminar LATCH heating prediction. There is excellent agreement between the nontripped results

Table 3 Orbiter incipient roughness results at $\alpha = 40$ deg in the LaRC 20-Inch Mach 6 Air Tunnel

		LATCH				SABLE	MINIVER	
Trips	Re_{inc} ($\times 10^6$)	θ, in.	δ, in.	Re_θ	Re_θ/M_e	Re_k	θ, in.	Re_θ/M_e
B2	1.6	0.00166	0.00923	57	67	163	0.00076	41
D1	3.8	0.00123	0.00685	105	114	165	0.00052	67
D2	1.9	0.00174	0.00960	72	79	189	0.00073	47
D3	1.0	0.00239	0.01330	54	59	158	0.00100	34
D4	0.8	0.00267	0.01478	48	52	N/A	0.00106	33
DE1	3.8	0.00172	0.00954	160	142	135	0.00063	83
DE2	1.9	0.00240	0.01330	110	98	162	0.00090	58
DE3	1.1	0.00312	0.01720	84	76	165	0.00114	46
DE4	0.8	0.00368	0.02049	73	65	N/A	0.00130	40
ECL1	3.1	0.00201	0.01153	168	142	93	0.0082	90
ECL2	1.9	0.00268	0.01490	132	110	144	0.00106	69
ECL3	1.1	0.00370	0.01937	102	85	150	0.00135	54
G1	3.1	0.00215	0.01215	203	162	96	0.00100	109
G2	1.6	0.00305	0.01690	144	115	122	0.00140	78
G3	1.1	0.00356	0.01980	122	97	156	0.00164	66

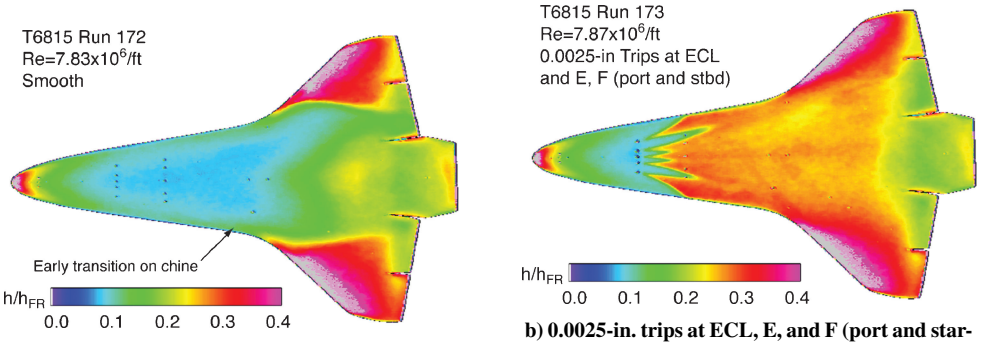

a) Smooth model

b) 0.0025-in. trips at ECL, E, and F (port and starboard)

Fig. 10 Comparison of smooth-body and tripped heating images for $Re = 7.8 \times 10^6$/ft.

and the laminar computations over the first half of the model. The experimental results also show a forward movement of natural transition as Reynolds number is increased. For the tripped case ($Re = 7.9 \times 10^6$/ft), the nonlaminar heating level quickly reaches a plateau that eventually matches (near the aft end of the model) with the nonlaminar heating level for the same Reynolds-number case without a trip, suggesting that turbulent heating levels have been reached. Figure 10 compares the heating images obtained for $Re = 7.8 \times 10^6$/ft, with and without trips. For the tripped case, an array of five trips ($k = 0.0025$ in.) across the $x/L = 0.258$ station at trip stations ECL and E, F (port and starboard) was used, as can be seen in Fig. 10b. Note the symmetry of the tripped flow and that turbulent flow covers over $\frac{3}{4}$ of the windward surface.

Based on the LATCH calculations, the onset of natural transition at $x/L = 0.61$ for $Re = 6.2 \times 10^6$/ft corresponds to Re_θ/M_e of roughly 290 and δ of 0.010 in. The height of the distributed roughness on the phosphor surface is on the order of 0.0005 in. nominally, with occasional isolated peaks on the order of 0.0015 in. Figure 10a is an example of a high-Reynolds-number smooth-model image, where tiny imperfections near the leading edge of the chine produces a small transition wedge that brings transition onset forward on the lower half of the image, thereby making transition appear slightly asymmetric. Along the centerline, however, the images show no evidence of surface imperfections. Therefore, the smooth model Re_θ/M_e value of 290 is believed to correspond to a distributed surface roughness to boundary-layer height ratio k/δ of 0.05. The smallest discrete roughness element ($k = 0.0025$ in.) is five times larger than the nominal background roughness and appears fully effective for $Re = 7.8 \times 10^6$/ft, as shown in Fig. 10b.

Transition Maps

To illustrate the systematic and well-behaved data of Ref. 3, transition onset, as identified from the point of departure from the laminar heating distributions along centerline, was plotted as a function of Reynolds number for each trip station and is shown in Fig. 11. A similar approach was used in Refs. 12, 29, and 30. The graphical presentation of results shown in these figures represent over 100 runs in the facility: from five trip stations along the model centerline, up to four trip heights at each station, and a minimum of five Reynolds numbers for each case. Each data point shown in Fig. 11 is the result of an individual run. For each Reynolds-number case, the resulting $(x/L)_{tr}$ value denotes whether the data indicated laminar, transitional, or fully turbulent flow downstream of the trip. For instance, a $(x/L)_{tr}$ value of 1 indicates that the trip had no effect (laminar), and a value corresponding to the trip location indicates a fully effective trip, whereas values in between represent a critical case. Previous studies[12,29,30] have shown that the curve representing the movement of transition as a function of Reynolds number is fairly smooth, and that distinctive sharp bends typically identify the start (incipient) and end (effective) points of transition movement. As shown in Fig. 11, the Reynolds-number increment often was too coarse to use a straight line between the data points to determine the incipient and effective values for the correlations to follow. Therefore, a smooth curve fit through the data was used to systematically define the bend in the curve that represents the incipient and effective points. For each trip case, the smooth curve was placed in a position that allowed the data points to fall within $\pm 10\%$ of the curve. The incipient and effective results obtained from Fig. 11 based on these smooth curves are listed in Tables 3 and 4, respectively, along with the corresponding calculated transition parameters.

Correlations

The primary objective of the present paper is to show the importance of using a consistent computational method when comparing different transition datasets. As stated earlier, Ref. 7 compared the orbiter[3] and X-33[4] results but did not account for the different

Table 4 Orbiter effective roughness results at $\alpha = 40$ deg in the LaRC 20-Inch Mach 6 Air Tunnel

		LATCH				SABLE	MINIVER	
Trips	Re_{eff} ($\times 10^6$)	θ, in.	δ, in.	Re_θ	Re_θ/M_e	Re_k	θ, in.	Re_θ/M_e
B2	2.2	0.00142	0.00791	70	80	241	0.00064	49
D1	5.2	0.00107	0.00590	125	135	250	0.00044	79
D2	2.5	0.00151	0.00840	86	93	274	0.00064	55
D3	1.6	0.00188	0.01040	67	73	265	0.00079	44
D4	1.3	0.00208	0.01160	62	67	N/A	0.00088	39
DE1	5.4	0.00142	0.00785	188	168	224	0.00053	99
DE2	2.7	0.00201	0.01120	136	121	270	0.00074	71
DE3	1.9	0.00240	0.01330	110	98	299	0.00090	58
DE4	1.3	0.00290	0.01603	93	83	N/A	0.00108	49
ECL1	5.0	0.00164	0.00913	216	181	178	0.00065	113
ECL2	2.8	0.00220	0.01220	158	134	258	0.00088	83
ECL3	1.8	0.00268	0.01490	132	110	280	0.00106	68
G1	4.8	0.00175	0.00969	252	201	180	0.00080	136
G2	2.4	0.00248	0.01374	179	143	222	0.00115	95
G3	1.8	0.00282	0.01570	155	124	295	0.00130	84

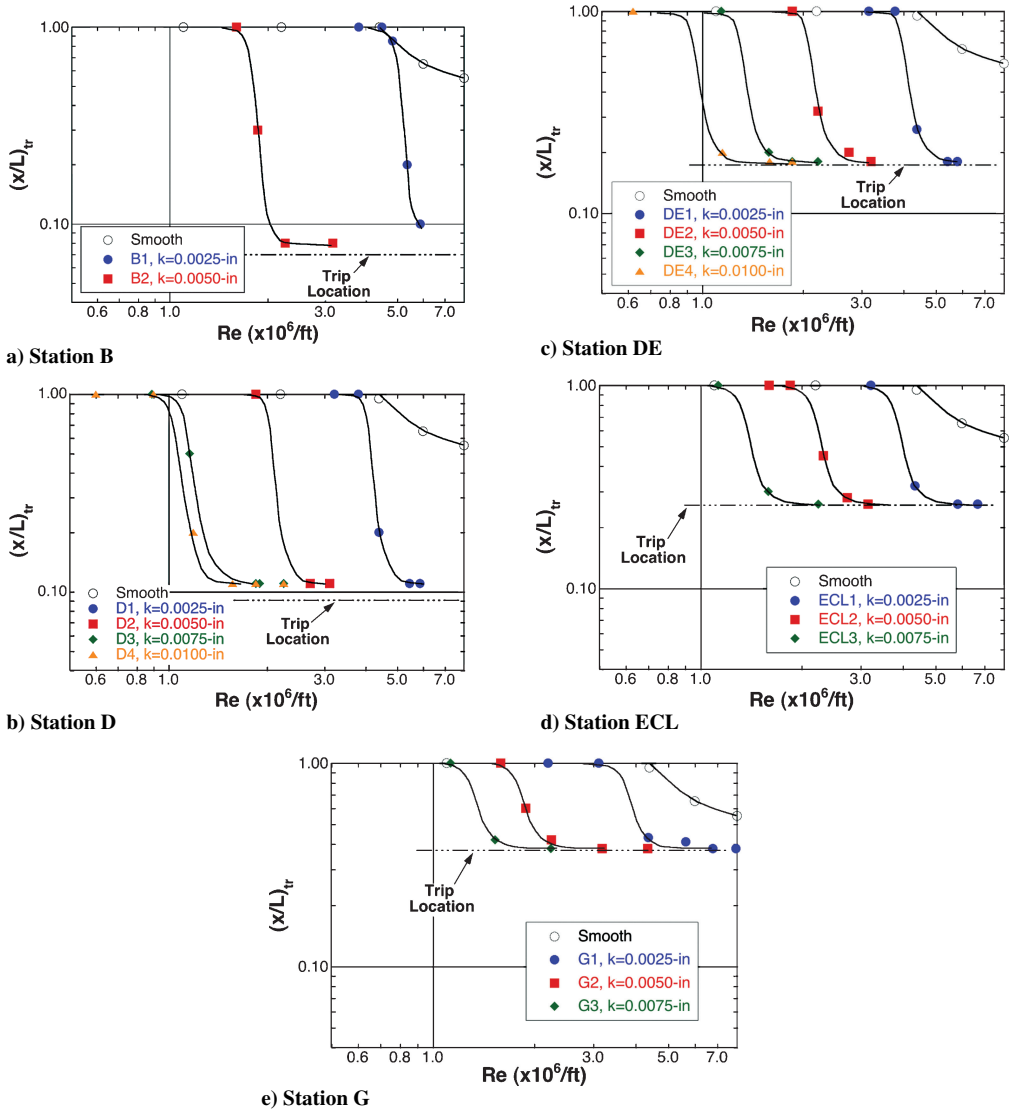

Fig. 11 Transition onset results along orbiter centerline.

codes used to predict edge properties. Figure 12 presents the effective transition data for the orbiter, recomputed with LATCH, as compared to the X-33[4] and X-38[5] results, using Re_θ/M_e as the transition parameter and k/δ as the disturbance parameter. The results are plotted in log–log coordinates, following Ref. 7. The results show that the data fall within ±20% of a straight-line representation of the power-law curve $(Re_\theta/M_e)(k/\delta) = 70$. This result represents the simplest correlation where the data can be fitted by a power-law curve with a −45-deg slope ($n = -1$) and thus suggests a one-to-one dependence of transition parameter to the selected disturbance parameter. The selection of an repeatability spread of ±20% of the curve fit was done to be consistent with the approach of Ref. 7. The key message from Fig. 12 is that when a consistent computational method is used, transition data sets that represent several different moderately blunt configurations at various angles of attack can be correlated simply by using properties based on edge conditions. This

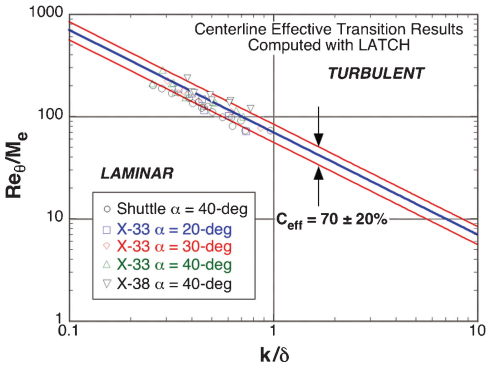

Fig. 12 Comparison of orbiter effective data computed with LATCH to X-33 and X-38 results.

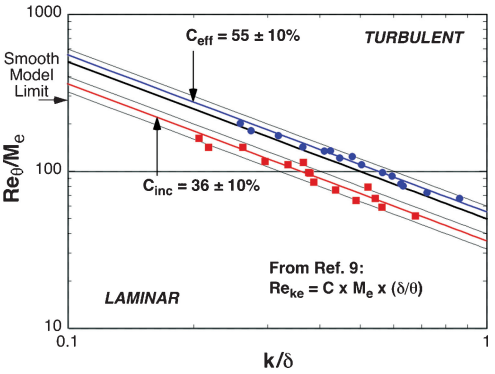

Fig. 13 Re_θ/M_e vs k/δ for orbiter.

fairly well-behaved and simple correlation appears universally applicable to moderately blunt lifting-body configurations in the same class of the orbiter, as long as a consistent computational approach is used to define and apply the correlation.

The correlation constant of 70 shown in Fig. 12 is comparable to the X-33 value ($C = 60$ for effective data), published in Ref. 4. However, the approach used to define the power-law curve through the X-33 data was slightly different, as the results were not represented by an average through the data, but rather a conservative line below the effective trends. In other words, a constant of 60 provides a curve by which over 95% of the X-33 data were shown to be fully effective. A similar conservative approach was used to define the incipient line, that is, 95% of the laminar data were below the incipient curve ($C = 45$). Further, in applying the X-33 discrete roughness transition results to the flight-vehicle design, additional conservatism was adopted whereby the incipient curve was used instead of the effective. As noted in Ref. 4, the flight criterion for transition was selected to be when Re_θ/M_e exceeded 250 at $x/L = 0.8$ on centerline; the entire windward surface was assumed turbulent. Based on the incipient curve, $Re_\theta/M_e = 250$ corresponds to a $k/\delta = 0.2$, which was used to define the allowable surface roughness. A conservative location (aft on the body) and transition onset value (based on the incipient curve) were used for design of the X-33 TPS. Until additional flight transition data are obtained to help reduce uncertainties with the extrapolation of wind-tunnel-derived correlations to flight, ultraconservative approaches will be required.

Figure 13 provides the orbiter results only based on LATCH using the same transition and disturbance parameters as Fig. 12, but now also including the incipient data. Both the incipient and effective trends are shown to fall within ±10% of the straight-line power-law curves of 36 and 55, respectively. By plotting these results with an uncertainty spread of ±10% (reduced from the ±20% used in Fig. 12), a very well-behaved correlation is shown. The smooth model limit, based on the noise levels associated with the present facility, is shown (although a k/δ of 0.05 is the more appropriate value for this limit).

In Ref. 7 the critical roughness Reynolds number associated with distributed data was suggested to be directly analogous to the effective Reynolds-number results for discrete trips. However, the appropriateness of using the effective value for discrete trips for a comparison to distributed results seems questionable. By definition for the distributed case, the critical roughness Reynolds number is based on local properties at the location of transition onset even though there might be a substantial run of distributed roughness ahead of transition. For the discrete case, the effective value of transition corresponds to when transition onset and the trip location are identical (or nearly so). Hypothetically, a second discrete trip could be placed some distance in front of the effective trip that is just large enough to be incipient, then the location of transition onset could just as likely be caused by the earlier incipient trip than the later effective trip. As noted in Ref. 9, when multiple trips (similar to distributed) have been tested, the results were similar to when a single trip was placed at the location of the initial trip. This would suggest that the transition onset location is dominated by the first significant trip and not the interaction of the multiple trips. Strictly speaking, trying to relate these two distinct data sets is problematic because of their basic definitions, as one is based on edge conditions at the trip location and the other is based on local conditions within the boundary layer at the location of transition. Nevertheless, the incipient value of discrete results might be more appropriate for comparison to distributed results because in both cases transition onset is occurring downstream of the initial location of roughness. Therefore, it is the opinion of the present authors that a better comparison is to use the incipient value for discrete and the critical value for distributed, especially in light of the preceding discussion regarding conservative approaches. Reference 7 discusses the algebraic manipulation of the power-law relation shown in Fig. 13 to obtain a roughness Reynolds number based on local edge conditions Re_{ke} that is equal to the curve constant C times the edge Mach number M_e times the shape factor δ/θ. Based on the incipient curve of 36, $M_e = 1.2$, and $\delta/\theta = 5.5$, $Re_{\text{ke}} = 240$ is obtained, which is significantly different from the orbiter value used in Ref. 7 (450 based on BLIMP).

Figure 14 provides the present orbiter results computed with LATCH using Re_θ/M_e for the transition parameter and k/θ for the disturbance parameter. Both the incipient and effective trends fall within ±10% of the straight-line power-law curves of 200 and 310, respectively. Again, by using an uncertainty spread of ±10%, a well-behaved correlation is indicated. A similar algebraic manipulation of the relation shown in Fig. 14 provides $Re_{\text{ke}} = C(M_e)$. Using the incipient curve of 200 and $M_e = 1.2$ yields $Re_{\text{ke}} = 240$. The similarity in results between these two plots should not be surprising considering that LATCH computes the boundary-layer thickness based solely on the shape factor, which would simply shift the results between the two figures. In hindsight, knowing that LATCH does not directly calculate δ, but instead uses an engineering relation with a constant more appropriate for flight, the correlation approach of Fig. 14 might have been preferable for X-33 and X-38, rather than Fig. 13. Again, the smooth model limit is shown (but is not implied to be at $k/\theta = 1$).

To investigate transition based on the critical roughness Reynolds number, Ref. 7 used the Dirling approach,[39] whereby the transition parameter is Re_θ and the disturbance parameter is $[\rho_k U_k k/\rho_e U_e \theta]$, which once the algebraic manipulation is performed

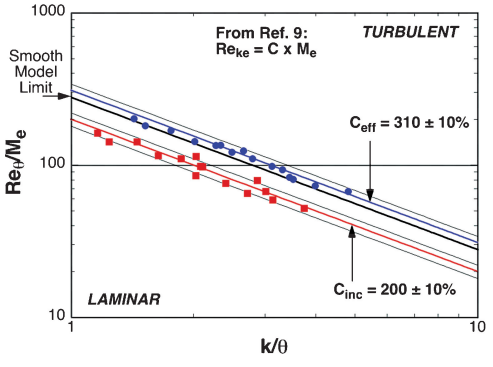

Fig. 14 Re_θ/M_e vs k/θ for orbiter.

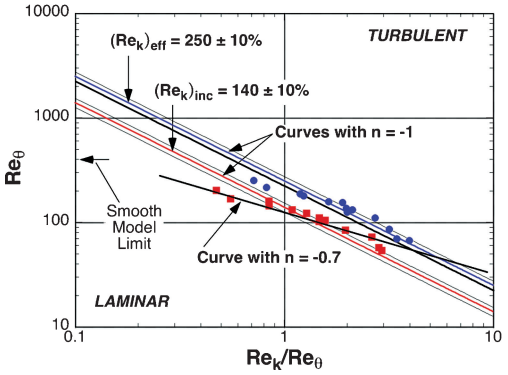

Fig. 15 Re_θ **vs** Re_k/Re_θ **for orbiter.**

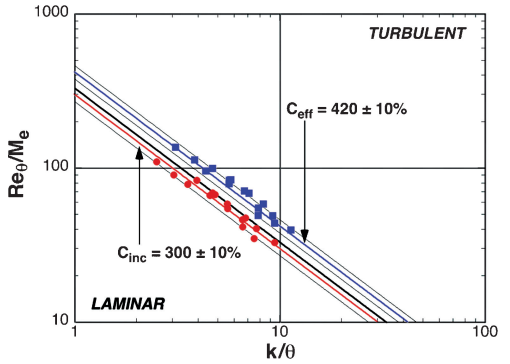

Fig. 16 Orbiter correlation based on MINIVER.

provides a roughness Reynolds number Re_k only if the assumption is made that $\mu_w = \mu_k$. As noted in Ref. 7, for adiabatic wall conditions and/or small roughness, this assumption is valid. However, because neither of these two conditions can be assumed for the present data set, the disturbance parameter was modified slightly to include the viscosity ratio between the boundary-layer edge and the top of the trip μ_e/μ_k. By including the viscosity terms, the disturbance parameter becomes Re_k/Re_θ. Thus, temperature effects within the boundary layer are included, which allows a Re_k correlation with fewer assumptions. Figure 15 provides the results when Re_θ is plotted as a function of Re_k/Re_θ. The incipient and effective data are plotted with straight-line power-law curves of 140 and 250, respectively. In this case, the uncertainty spread of ±10% does not capture all of the data, indicating a less well-behaved correlation. In fact the slope of the data appears to follow a trend, as shown, whose curve would have an exponent of −0.7, coincidentally the same exponent used with the PANT correlation,[40] which is fairly similar in form and includes the edge-to-wall temperature ratio. Apparently by including the viscosity (temperature) terms, the critical roughness Reynolds number approach of Dirling departs from the ideal curve ($n = -1$). However, it should be noted that the previous ballistic range Re_k values presented in Ref. 7 are for distributed roughness, where the results are evaluated at the location of transition onset and not at the discrete trip location as was done here. The incipient straight-line curve shown (exponent of 1) provides a roughness Reynolds number Re_k of 140. Using the Re_k and Re_{ke} values obtained from the present investigation, based on incipient curves and the LATCH and SABLE computations, provides values roughly half those presented in Ref. 7. For comparison, if the effective curves had been used, the Re_k and Re_{ke} values would still have been 25% lower than Ref. 7. This result indicates the sensitivity of correlating approaches to the assumptions and codes used and emphasizes the potential error from comparing results from different studies without carefully considering the details of the computational method used.

The preceding results show that when a consistent computational method is used a simple correlation based on edge conditions can be used to predict transition in the wind tunnel over the entire windward surface for several configurations at various angles of attack. Qualitatively, it also appears that these methods can be used to predict transition behavior on the orbiter in flight.[2] This will be of interest to vehicle designers who tend to use simple approximate methods, such as the MINIVER[14] code, to compute convective heating rates and edge conditions for predicting transition onset along proposed trajectories and subsequently trajectory tailoring to minimize turbulent heat loads. In an effort to provide vehicle designers a precalibrated correlation method, the present orbiter transition onset results were used to generate a MINIVER correlation curve using Re_θ/M_e for the transition parameter and k/θ for the disturbance parameter, and the results are presented in Fig. 16. The results show a well-behaved correlation with the results shifted roughly 50% higher compared to the LATCH results. Obviously, a correlation curve that shifts so dramatically, based on the computational approach used, is further evidence of the importance of utilizing a consistent approach when applying correlations to future programs.

Clearly the use of a consistent computational method is critical when comparing results from different studies. The present results have shown that the correlation curves can vary by as much as 50% or more based on the code that was used to develop the curves. Reference 7 used several published transition data sets, all based on different computational methods, to imply that had the X-33 flown; the resulting "transition performance might well have been outside the design envelope." However, the uncertainty band associated with the critical roughness Reynolds numbers used to support that view is now shown to be greater than ±50%, which is to say that those comparisons have little merit. The values calculated here, using the appropriate edge Mach numbers and shape factor, for isolated, incipient, three-dimensional roughness are drastically different (Re_k of 140 and Re_{ke} of 240 vs 344 and 1050, respectively, from Ref. 7).

Conclusions

Results from a previous experimental investigation of discrete roughness transition on the Space Shuttle Orbiter performed in the NASA LaRC 20-Inch Mach 6 Air Tunnel has been reanalyzed. Phosphor thermography was used to provide global heating images of the windward surface and to assess the state of the boundary layer. The discrete roughness elements were systematically varied in size and location along the centerline of 0.0075-scale models at an angle of attack of 40 deg. The resulting roughness transition results were computed with the LATCH code using the same approach and assumptions that had been used for previously published X-33 and X-38 results. The comparison shows that when a consistent approach is used, transition data sets, representing several configurations at various angles of attack, collapse into a well-behaved correlation based on edge properties. The resulting correlation curves based on LATCH were roughly double the earlier published orbiter curves based on BLIMP. Also, the orbiter transition results were computed and correlated using the MINIVER code to provide precalibrated correlation curves for use in vehicle design; the results are a further 50% higher than the present LATCH curves. The present results clearly show the critical importance of using a consistent computational method when applying the transition correlation curves to vehicle design. For future designs of TPS systems, the present experimental data can be used to calibrate the preferred computational method of the vehicle designers.

References

[1]Haney, J. W., "Orbiter Entry Heating Lessons Learned from Development Flight Test Program," *Shuttle Performance: Lessons Learned*, NASA CP-2283, Pt. 2, 1983, pp. 719–751.

[2]Bouslog, S. A., Bertin, J. J., Berry, S. A., and Caram, J. M., "Isolated Roughness Induced Boundary-Layer Transition: Shuttle Orbiter Ground Tests and Flight Experience," AIAA Paper 97-0274, Jan. 1997.

[3]Berry, S. A., Bouslog, S. A., Brauckmann, G. J., and Caram, J. M., "Shuttle Orbiter Experimental Boundary-Layer Transition Results with Isolated Roughness," *Journal of Spacecraft and Rockets*, Vol. 35, No. 3, 1998, pp. 241–248.

[4]Berry, S. A., Horvath, T. J., Hollis, B. R., Thompson, R. A., and Hamilton, H. H., "X-33 Hypersonic Boundary Layer Transition," *Journal of Spacecraft and Rockets*, Vol. 38, No. 5, 2001, pp. 646–657; also AIAA Paper 99-3560, June 1999.

[5]Horvath, T. J., Berry, S. A., Merski, N. R., and Fitzgerald, S. M., "X-38 Experimental Aerothermodynamics," *Journal of Spacecraft and Rockets*, Vol. 41, No. 2, 2004, pp. 272–292; also AIAA Paper 2000-2685, June 2000.

[6]Hamilton, H. H., II, Greene, F. A., and DeJarnette, F. R., "Approximate Method for Calculating Heating Rates on Three-Dimensional Vehicles," *Journal of Spacecraft and Rockets*, Vol. 31, No. 3, 1994, pp. 345–354.

[7]Reda, D. C., "Review and Synthesis of Roughness-Dominated Transition Correlations for Reetry Applications," *Journal of Spacecraft and Rockets*, Vol. 39, No. 2, 2002, pp. 161–167.

[8]Stetson, K. F., "Comments on Hypersonic Boundary-Layer Transition," U.S. Air Force Wright Research and Development Center, WRDC-TR-90-3057, Wright–Patterson AFB, OH, Sept. 1990.

[9]Chrusciel, G. T., "Active and Passive Boundary Layer Tripping," AIAA Paper 97-2016, June 1997.

[10]Bouslog, S. A., An, M. Y., Campbell, C. H., Wang, K. C., and Pelley, R. L., "Orbiter Boundary-Layer Transition Working Group: Analysis and Ground Test Status Report," NASA Johnson Space Center, JSC-26812, Oct. 1994.

[11]Batt, R. G., and Legner, H. H., "A Review of Roughness-Induced Nosetip Transition," *AIAA Journal*, Vol. 21, No. 1, 1983, pp. 7–22.

[12]Van Driest, E. R., and Blummer, C. B., "Boundary Layer Transition on Cones and Spheres at Supersonic Speeds—Effects of Roughness and Cooling," U.S. Air Force Office of Scientific Research, Rept. 67-2048, Anaheim, CA, July 1967.

[13]Berkowitz, A. M., Kyriss, C. L., and Martellucci, A., "Boundary Layer Transition Flight Test Observations," AIAA Paper 77-125, Jan. 1977.

[14]Engel, C. D., and Praharaj, S. C., "Miniver Upgrade for the AVID System, Vol. I: LANMIN User's Manual," NASA CR-172212, Aug. 1983.

[15]Kleb, W. L., Wood, W. A., Gnoffo, P. A., and Alter, S. J., "Computational Aeroheating Predictions for X-34," *Journal of Spacecraft and Rockets*, Vol. 36, No. 2, 1999, pp. 179–188.

[16]Riley, C. J., Kleb, W. L., and Alter, S. J., "Aeroheating Predictions for X-34 Using an Inviscid Boundary-Layer Method," *Journal of Spacecraft and Rockets*, Vol. 36, No. 2, 1999, pp. 206–215.

[17]Wurster, K. E., Riley, C. J., and Zoby, E. V., "Engineering Aerothermal Analysis for X-34 Thermal Protection System Design," *Journal of Spacecraft and Rockets*, Vol. 36, No. 2, 1999, pp. 216–228.

[18]Tartabini, P. V., Wurster, K. E., Korte, J. J., and Lepsch, R. A., "Multidisciplinary Analysis of a Lifting Body Launch Vehicle," *Journal of Spacecraft and Rockets*, Vol. 39, No. 5, 2002, pp. 788–795.

[19]Miller, C. G., "Langley Hypersonic Aerodynamic/Aerothermodynamic Testing Capabilities—Present and Future," AIAA Paper 90-1376, June 1990.

[20]Merski, N. R., "Reduction and Analysis of Phosphor Thermography Data with the IHEAT Software Package," AIAA Paper 98-0712, Jan. 1998.

[21]Buck, G. M., "Automated Thermal Mapping Techniques Using Chromatic Image Analysis," NASA TM 101554, April 1989.

[22]Buck, G. M., "Surface Temperature/Heat Transfer Measurement Using a Quantitative Phosphor Thermography System," AIAA Paper 91-0064, Jan. 1991.

[23]Micol, J. R., "Aerothermodynamic Measurement and Prediction for a Modified Orbiter at Mach 6 and 10 in Air," *Journal of Spacecraft and Rockets*, Vol. 32, No. 5, 1995, pp. 737–748.

[24]Hollis, B. R., Horvath, T. J., Berry, S. A., Hamilton, H. H., and Alter S. A., "X-33 Computational Aeroheating Predictions and Comparisons with Experimental Data," *Journal of Spacecraft and Rockets*, Vol. 38, No. 5, 2001, pp. 658–669; also AIAA Paper 99-3559, June 1999.

[25]Loomis, M. P., Venkatapathy, E., Papadopoulos, P., Davies, C. B., Berry, S. A., Horvath, T. J., and Campbell, C. H., "Aeroheating and Aerodynamic CFD Validation and Prediction for the X-38 Program," AIAA Paper 97-2478, June 1997.

[26]Buck, G. M., and Vasquez, P., "An Investment Ceramic Slip-Casting Technique for Net-Form, Precision, Detailed Casting of Ceramic Models," U.S. Patent 5,266,252, 30 Nov. 1993.

[27]Bertin, J. J., Stetson, K. F., Bouslog, S. A., and Caram, J. M., "Effect of Isolated Roughness Elements on Boundary-Layer Transition for Shuttle Orbiter," *Journal of Spacecraft and Rockets*, Vol. 34, No. 4, 1997, pp. 426–436.

[28]Bertin, J. J., Hayden, T. E., and Goodrich, W. D., "Shuttle Boundary-Layer Transition due to Distributed Roughness and Surface Cooling," *Journal of Spacecraft and Rockets*, Vol. 19, No. 5, 1982, pp. 389–396.

[29]Boudreau, A. H., "Artificially Induced Boundary-Layer Transition on Blunt-Slender Cones at Hypersonic Speeds," *Journal of Spacecraft and Rockets*, Vol. 16, No. 4, 1979, pp. 245–251.

[30]Pate, S. R., "Dominance of Radiated Aerodynamic Noise on Boundary-Layer Transition in Supersonic-Hypersonic Wind Tunnels," Arnold Engineering Development Center, TR-77-107, Arnold Air Force Station, TN, March 1978.

[31]Fay, J. A., and Ridell, F. R., "Theory of Stagnation Point Heat Transfer in Dissociated Air," *Journal of Aeronautical Sciences*, Vol. 25, No. 2, 1958, pp. 73–85.

[32]Gnoffo, P. A., "An Upwind-Biased, Point-Implicit Relaxation Algorithim for Viscous, Compressible Perfect-Gas Flow," NASA TP-2953, Feb. 1990.

[33]Anderson, J. D., Jr., *Hypersonic and High Temperature Gas Dynamics*, McGraw–Hill, New York, 1989, p. 296.

[34]Zoby, E. V., Moss, J. N., and Sutton, K., "Approximate Convective-Heating Equations for Hypersonic Flows," *Journal of Spacecraft and Rockets*, Vol. 18, No. 1, 1981, pp. 64–70.

[35]Cohen, C. B., and Reshotko, E., "The Compressible Laminar Boundary Layer with Heat Transfer and Arbitrary Pressure Gradient," NACA Rept. 1294, 1956.

[36]Hamilton, H. H., II, Millman, D. R., and Greendyke, R. B., "Finite-Difference Solution for Laminar or Turbulent Boundary Layer Flow over Axisymmetric Bodies with Ideal Gas, CF_4, or Equilibrium Air Chemistry," NASA TP-3271, Dec. 1992.

[37]An, M. Y., Wang, K. C., and Tam, L. T., "Computation of Inviscid Flow Field Around 3-D Aerospace Vehicles and Comparison with Experimental & Flight Data," AIAA Paper 93-0885, Jan. 1993.

[38]Wang, K. C., "An Axisymmetric Analog Two-Layer Convective Heating Procedure with Application to the Evaluation of Space Shuttle Orbiter Wing Leading Edge and Windward Surface Heating," NASA CR 188343, Sept. 1994.

[39]Dirling, R. B., Jr., Swain, C. E., and Stokes, T. R., "The Effect of Transition and Boundary Layer Development on Hypersonic Reentry Shape Change," AIAA Paper 75-673, May 1975.

[40]Stetson, K. F., "Boundary-Layer Transition on Blunt Configurations," NASA Johnson Space Center, JSC-26528, Feb. 1994.

R. Kimmel
Associate Editor

Color reproductions courtesy of NASA Langley Research Center.